ELSEVIER

Journal of Molecular Catalysis A: Chemical 167 (2001) 33–46

JOURNAL OF MOLECULAR CATALYSIS A: CHEMICAL

www.elsevier.com/locate/molcata

Single crystal and high area titania supported rhodium: the interaction of supported $Rh(CO)_2$ with NO

Brian E. Hayden*, Alex King[1], Mark A. Newton, Naruo Yoshikawa

Department of Chemistry, University of Southampton, Highfield, Southampton SO17 1BJ, UK

Received 9 May 2000

Abstract

Model Rh/TiO_2 catalysts have been prepared by metal organic chemical vapour deposition (MOCVD) of $[Rh(CO)_2Cl]_2$ to $TiO_2(1\,1\,0)$ and high area (Degussa P25) powder TiO_2 samples. The rhodium geminal dicarbonyl species ($Rh(CO)_2$) is produced on each surface, and the reaction of the supported $Rh(CO)_2$ with NO has been studied using FT-RAIRS, transmission FT-IR and XPS.

$TiO_2(1\,1\,0)$–$Rh(CO)_2$ is converted by exposure to NO at 300 K solely to a highly dispersed $Rh(NO)^+$ species with ν(N–O) observed as a transmission band in FT-RAIRS at 1920 cm^{-1}. This species is thermally more stable than the geminal dicarbonyl species, and XPS measurements indicate that the NO is removed without the formation of adsorbed nitrogen residues by 600 K. Re-exposure to CO results in the complete regeneration of $TiO_2(1\,1\,0)$–$Rh(CO)_2$ from $TiO_2(1\,1\,0)$–$Rh(NO)^+$. TiO_2(P25)–$Rh(CO)_2$ is present in a variety of surface environments, with broad bands observed at the same frequencies as for $TiO_2(1\,1\,0)$–$Rh(CO)_2$ (ν_{sym}(C–O) = 2110 cm^{-1} and ν_{asym}(C–O) = 2030 cm^{-1}). Exposure of TiO_2(P25)–$Rh(CO)_2$ to NO at 300 K results in the formation of TiO_2(P25)–$Rh(NO)^+$ with ν(N–O) at 1920 cm^{-1}, and TiO_2(P25)–Rh(CO)(NO) with ν(N–O) at 1750 cm^{-1} and ν(C–O) at 2110 cm^{-1}.

TiO_2(P25)–Rh^0 clusters, formed through the thermal decomposition of TiO_2(P25)–$Rh(CO)_2$ at various temperatures, react with NO to produce additional surface nitrosyl species. On a surface heated to 380 K where TiO_2(P25)–$Rh(CO)_2$ decarbonylation has only just taken place, reaction with NO at 300 K results in the formation of the same species as those produced through the reaction of TiO_2(P25)–$Rh(CO)_2$ directly NO, i.e. (TiO_2(P25)–$Rh(NO)^+$) and TiO_2(P25)–Rh(CO)(NO). Re-exposure of this surface to CO results in the complete reconversion of the dispersed nitrosyl to TiO_2(P25)–$Rh(CO)_2$. When larger clusters are formed on a surface by heating to 650 K, reaction with NO leads initially to the adsorption of linear and bridged bound NO on TiO_2(P25)–Rh^0 with respective ν(N–O) bands observed in the IR at 1818 and 1680 cm^{-1}. Further exposure of NO, however, results in the complete disruption of the TiO_2(P25)–Rh^0 clusters. This is evidenced by the disappearance of the bridging and linear bands and the appearance of a strong band associated with ν(N–O) of TiO_2(P25)–$Rh(NO)^+$ at 1920 cm^{-1}, and bands at 1745 and 1550 cm^{-1} assigned to dispersed TiO_2(P25)–$Rh(NO)^-$ and TiO_2(P25)–$Rh(NO_2)^-/(NO_3)^-$. The latter species we suggest are stabilised by surface defects such as oxygen vacancies which may have been formed during the clustering of the Rh^0. After thermal treatment to temperatures of 800 K, where

*Corresponding author. Tel.: +44-23-8059-2776; fax: +44-23-8059-3781.
E-mail address: b.e.hayden@soton.ac.uk (B.E. Hayden).
[1]Present address: BP Chemicals, Chertsey Road, Sunbury on Thames, Middlesex TW16 4LN, UK.

PII: S1381-1169(00)00488-X

encapsulation of the TiO_2(P25)–Rh^0 clusters should occur, we see a strong suppression of NO adsorption on the clusters. Nevertheless disruption of clusters still takes place with the formation of TiO_2(P25)–$Rh(NO)^-$ even under these (SMSI) conditions.

Keywords: Rhodium; $Rh(CO)_2$; NO

1. Introduction

The importance of supported Rh systems to the chemical industry is well known; a number of both homogeneous and heterogeneous industrial processes are mediated using some form of Rh [1]. In each case the exact form of the Rh can have a significant bearing on the performance of these catalysts. It is known, for instance, that the dispersion of Rh in supported heterogeneous catalysts can have a bearing on the reactivity and selectivity of these catalysts for a given reaction. It is also known that this parameter is sensitive to the precursor used in the preparation of the final catalyst [2–5]. Probing the details of the relationship between the characteristics that a catalyst displays, and the phase and/or dispersion of the active metal component is therefore of considerable interest.

One of the many problems that are encountered in analysing these processes in a detailed manner is the initial non-uniformity of the real system. Ideally one would like to remove all of the initial distributions of sites and particles sizes and begin with a system that is uniform; but nonetheless retains the essential character of the real catalyst. Though metal single crystals match this criterion in some respects this approach is rooted in the limit of very low dispersion. Typical supported Rh based systems exhibit a tendency to form small particles of intrinsically high dispersion. Also, the use of metal single crystals in modelling supported metal chemistry implicitly assumes that the support itself does not modify the behaviour.

In the case of supported Rh systems a number of investigators have found that a situation similar to that described above can be achieved for low loaded (<2 wt.%) Rh/Al_2O_3 catalysts from a $RhCl_3$ precursor [4,6–10]. This, when reduced and then exposed to CO, results in a catalyst that is predominately comprised of $Rh^I(CO)_2$ species. In the case of the Rh/TiO_2 system, it has also been shown that MOCVD of $[Rh(CO)_2Cl]_2$ onto a single crystal substrate [11–16] generates a uniform, mono-dispersed, layer of $Rh(CO)_2$. The thermal chemistry of this well-defined system [13], interaction with hydrogen [14,15], and the orientational alignment of the geminal dicarbonyl [16] species on TiO_2(1 1 0) surface have been investigated in detail.

Moreover by considering the saturation coverage of the $Rh(CO)_2Cl$ derived from single crystal measurements [13], and the surface area of the Degussa P25 ($\sim 50\,m^2\,g^{-1}$) we can estimate that at saturation we should be able to produce a mono-disperse Rh^I system at metal loadings approaching 5 wt.%; this is a considerably higher loading than is usually used to form essentially mono-disperse Rh catalysts [6–10]. Thus, MOCVD of $[Rh(CO)_2Cl]_2$ potentially allows the investigation of mono-disperse Rh species over a wider range of metal loadings than is possible from conventional wet chemistry techniques.

The principal aims of auto exhaust catalysis are to effect efficient conversion of CO and NO_x to CO_2 and N_2 and to remove hydrocarbons from exhaust fumes. The net reactions at work in the former stages are:

$$2NO + 2CO \Rightarrow N_2 + 2CO_2 \quad (1)$$

$$2NO + CO \Rightarrow N_2O + CO_2 \quad (2)$$

It should be noted that $[Rh(CO)_2Cl]^-$ is an active species for the homogeneous facilitation of reaction (2) [17].

In heterogeneous systems these reactions have been shown to be dispersion and temperature dependant behaviour. On small Rh particles the reaction

$$NO_a \Rightarrow N_a + O_a \quad (3)$$

appears to become rate limiting due to the low number of the appropriate ensembles of Rh atoms available to affect dissociation; as the particles become larger this restriction to NO dissociation, and therefore NO_x conversion, is relieved [18]. Particle size also affects the recombination of N_a to form N_2 [19].

$$2N_a \Rightarrow N_{2(g)} \quad (4)$$

Decreasing particle size increases the temperature at which this process occurs.

Numerous studies have previously investigated the interaction of CO and NO on high area supported Rh catalysts [20–28]. On typical high area catalysts, with a variety of particulate and mono-dispersed Rh, the adsorption of NO leads to the formation of a number of species: $Rh(NO)^+$, Rh(NO), $Rh(NO)^-$, and $Rh(NO)_2$, have all been identified. The formal charges ascribed to the $Rh(NO)^+$ and $Rh(NO)^-$ should not be interpreted too literally, and the nomenclature is only used because of its extensive application in the literature. Co-adsorption of CO and NO have also resulted in the observation of isocyanate species and/or the mono-disperse Rh(NO)(CO). Which species are seen depends on the treatment of the Rh in the catalyst; as a result of this both $Rh(CO)_2$ and $Rh(NO)^+$ have been associated with the same site for Rh/SiO_2 systems [21]. NO has also been shown to affect the dispersion of the Rh phase in its own right, promoting the disruption of Rh clusters and, in the presence of CO, promoting the formation of the mono-disperse $Rh(CO)_2$ species [21–23].

UHV studies on Rh single crystals have pointed to a preference for bridge bonded NO adsorption (see Table 1) on clean Rh surfaces [29–31]. This assignment has recently been called into question, with temperature programmed static-SIMS [32], core-level X-ray photoelectron diffraction (XPD) [33] and theoretical calculations [34] suggesting that hollow sites (ν(N–O) $\sim$ 1640, ..., 1544 cm^{-1}) may be more likely. Also, a site switching effect has been shown for NO adsorption to an oxygen pre-covered surface such that the more highly co-ordinated NO species shift into linear sites at just below room temperature [35].

A summary of transmission IR frequencies used to identify a number of pertinent CO and NO containing species (on both high area and single crystal systems) is given in Table 1.

Table 1
Infra red absorption frequencies reported for $Rh(CO)_x$ and $Rh(NO)_x$ species observed on high area supported Rh catalysts and TiO_2 single crystals

Adsorbed species	Vibrationalmode	Frequency (cm^{-1})	Support and reference
$Rh_2(CO)$ bridge	ν(C–O)	1900–1830	Al_2O_3 [20], SiO_2 [21], TiO_2[1 1 0] [13],
$Rh_x(CO)$ (x_2) linear	ν(C–O)	2020–2090	Al_2O_3 [20], SiO_2 [21,22], TiO_2 [22], TiO_2[1 1 0] [13]
$Rh_2(CO)_3$ (bridge)	ν(C–O)	1818	Al_2O_3 [37–38]
$Rh_2(CO)_3$ (linear)	ν(C–O)	1987	Al_2O_3 [37–38]
$Rh(CO)_2$	ν_{sym}(C–O)	2108, 2112	Al_2O_3 [20,24–28], SiO_2 [21–23], TiO_2 [22] TiO_2[1 1 0] [11–16]
$Rh(CO)_2$	ν_{asym}(C–O)	2040, 2030	Al_2O_3 [20,24–28], SiO_2 [21–23], TiO_2 [22], TiO_2[1 1 0] [11–16]
$Rh(NO)^+$	ν(N–O)	1910–1930	Al_2O_3 [20,24–28], SiO_2 [21–23], TiO_2 [22]
$Rh(NO)_2$	ν_{sym}(N–O)	1830–1820	Al_2O_3 [20,25,27], SiO_2 [23], zeolite-Y [47]
$Rh(NO)_2$	ν_{asym}(C–O)	1740	Al_2O_3 [20,25,27], SiO_2 [23], zeolite-Y [47]
Rh(NO)(CO)	ν(C–O)	2101	Al_2O_3 [20,25,26]
Rh(NO)(CO)	ν(N–O)	1755	Al_2O_3 [20,25,26]
Rh(NO)	ν(N–O)	1830	Al_2O_3 [20,25,28]
Rh(NO) (linear)	ν(N–O)	1840, 1800–1850	O/Rh[1 1 1] [35], theory [34]
Rh(NO)	ν(N–O)	1770–1710	Al_2O_3 [20,25–28], SiO_2 [21,22],
Rh(NO)	ν(N–O)	1650–1660	Al_2O_3 [20,28], SiO_2 [21,22]
$Rh_2(NO)$ (bridge)	ν(N–O)	1630, 1560–1710, 1580–1680, 1644–1690	Rh[1 1 1] [29], Rh[1 1 0] [30], Rh[1 0 0] [31], theory [34]
Rh_3NO (hollow)	ν(N–O)	1544–1643	Theory [34]
(NCO)		2260, 2235	Al_2O_3 [25,26,28], SiO_2 [21]
N_2O	ν(N–O)	2225	Al_2O_3 [25,26], SiO_2 [21]
CO_3^{2-}	ν(C–O)	1385, 1440, 1580	Al_2O_3 [26]
NO_2 or NO_3^-	ν(N–O)	1550	Al_2O_3 [26], SiO_2 [23]

2. Experimental

Single crystal experiments were carried out in a stainless steel UHV chamber (base pressure $\sim 1 \times 10^{-9}$ mbar) equipped with XPS, FT-RAIRS, and LEED facilities; this equipment has been described previously [14]. FT-RAIRS experiments utilised an InSb detector with a spectral cut off at 1800 cm^{-1}.

The (1 1 0) oriented TiO_2 was mounted in a Ta boat and resistively heated via two 0.3 mm W wires spot welded to the boat; the sample temperature was measure using a chromel–alumel thermocouple also spot welded to the boat. Because of the size of the TiO_2(1 1 0) crystals temperatures recorded in this manner should be regarded at overestimates of the true surface temperature. In the experiments shown in this paper, where heating of the single crystal is made to effect reactions at relatively low temperature, the over estimate of surface temperature should be ~25 K.

The surface was prepared by ion bombardment (~2 keV, 2 h, 800 K) followed by annealing (2 h, 1000 K), and finally cooling slowly in oxygen (1×10^{-7} mbar). $[Rh(CO)_2Cl]_2$ was purified in the manner described previously [13–16]. NO and CO were dosed directly into the system via fine leak valves.

The transmission IR experiments on the high area titania were carried out in a diffusion pumped stainless steel vacuum chamber. The design concept was similar to that in systems employed elsewhere [27,36–38]. The reaction cell slides in and out of the IR spectrometer using a moveable table on which the UHV system is mounted so that the chamber may be baked outside of the environment of the IR spectrometer. The UHV system was equipped with a mass spectrometer, ion gauge, and gas dosing facilities. Transmission of the IR beam through the IR cell was facilitated by two KBr windows mounted either side of the sample and in this case detection was made using an MCT detector with a spectral cut off ~800 cm^{-1}. The high area TiO_2 powder (Degussa P25) was suspended in acetone and sprayed onto an 80% transmission Ni mesh using an airbrush. The Ni mesh was then clamped between two posts that supplied power for the resistive heating of the mesh (up to 1000 K) and cooling to ~150 K. Temperature was measured using a chromel–alumel thermocouple spot welded into the Ni mesh. After baking base pressures of $<1 \times 10^{-8}$ mbar were routinely achieved. Prior to MOCVD the TiO_2 was heated to ~500 K in order to remove surface hydroxyl species. Even under high vacuum, however, IR measurements showed that (over the time scales of the order of the reactions we are considering here) the TiO_2 sample showed evidence of some growth of a broad hydroxyl absorption band.

3. Results

3.1. IR spectra of TiO_2(1 1 0)–$Rh(CO)_2$ and high area TiO_2(P25)–$Rh(CO)_2$

Fig. 1 shows the IR spectra derived from MOCVD of $[Rh(CO)_2Cl]_2$ to the Degussa P25 TiO_2. The spectra show the two characteristic IR active modes associated with the symmetric (ν_{sym}(C–O)) ~ 2110 cm^{-1}) and asymmetric (ν_{asym}(C–O)) ~ 2030 cm^{-1}) stretches of the adsorbed $Rh(CO)_2$ species (Table 1).

The corresponding FT-RAIRS spectrum for room temperature adsorption of $[Rh(CO)_2Cl]_2$ to TiO_2(1 1 0), and its physical origins, has been described previously [13,16] and is thus omitted here. It is characterised by the symmetric (ν_{sym}(C–O)) ~ 2112 cm^{-1}) and asymmetric (ν_{asym}(C–O)) ~ 2030 cm^{-1}) stretches of the adsorbed $Rh(CO)_2$ species observed as transmission and absorption bands, respectively. The IR spectrum derived from the high area TiO_2 powder shows the same major features though

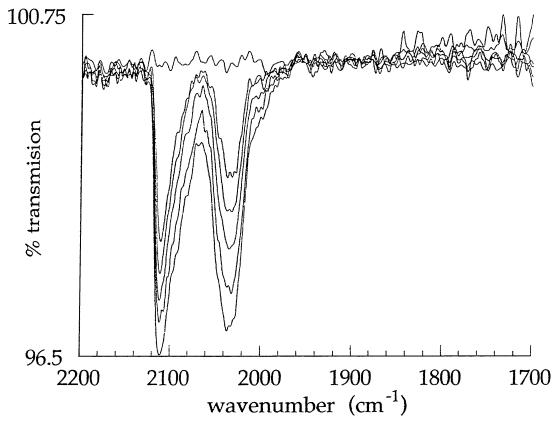

Fig. 1. Transmission IR spectra TiO_2(P25)–$Rh(CO)_2$ species produced at 300 K by dissociative adsorption of $[Rh(CO)_2Cl]_2$ on Degussa P25 TiO_2.

there are differences with respect to the single crystal case. Most notable is the increased broadness of the spectral features and the presence of fine structure within them. This is primarily due to a heterogeneity of adsorption sites associated with the mono-disperse $Rh(CO)_2$. This is not entirely surprising given that both anatase and rutile phases are present in this high area titania powder sample, and that for each phase a variety of crystal planes will be present in the sample.

3.2. The reaction of NO with TiO_2(1 1 0)–$Rh(CO)_2$

Fig. 2 shows a series of FT-RAIRS spectra obtained while exposing TiO_2(1 1 0)–$Rh(CO)_2$ to NO at 300 K. $Rh(CO)_2$ has been produced by the dissociative adsorption of the rhodium carbonyl chloride and a new IR background taken before NO exposure; removal of the symmetric gem-dicarbonyl (transmission) band therefore results in an adsorption, and an absorption/transmission band is expected at the frequency associated with the asymmetric feature [16]. We can see that immediately the NO is introduced we observe the loss of the TiO_2(1 1 0)–$Rh(CO)_2$ species. As the reaction proceeds we observe the appearance of a transmission band at $\sim$1920 cm^{-1}. Eventually the attenuation of the adsorption features due to the geminal dicarbonyl is complete, indicating that this species has been removed from the surface. The frequency of the new vibration is indicative of the formation of a TiO_2(1 1 0)–$Rh(NO)^+$ species with ν(N–O) $\sim$ 1920 cm^{-1} (Table 1). The fact that the resonance is a transmittance feature also tells us that the Rh in this species is very highly dispersed. It can only result from the coupling of a normal polarised mode to the normal component of the p-polarised radiation at the titania dielectric [11–16,39]. If the band were a result of NO species on large Rh particles, the dielectric response of the metal would dominate the IR process resulting in an absorption band [13,39]. If the gem-dicarbonyl is exposed to NO at 375 K, one obtains the same result as that shown in Fig. 2, but at $\sim$1/5 of the NO exposure required for complete conversion at 300 K. We find that exposing the TiO_2(1 1 0)–$Rh(NO)^+$ species to CO (1×10^8 L) at 375 K results in complete regeneration of the TiO_2(1 1 0)–$Rh(CO)_2$ species; regeneration is also slower at 300 K. It is evident that the rates of NO reaction with the gem-dicarbonyl, and the subsequent rate of regeneration from the TiO_2(1 1 0)–$Rh(NO)^+$ adduct, are very different; the latter reaction being considerably more difficult than the former.

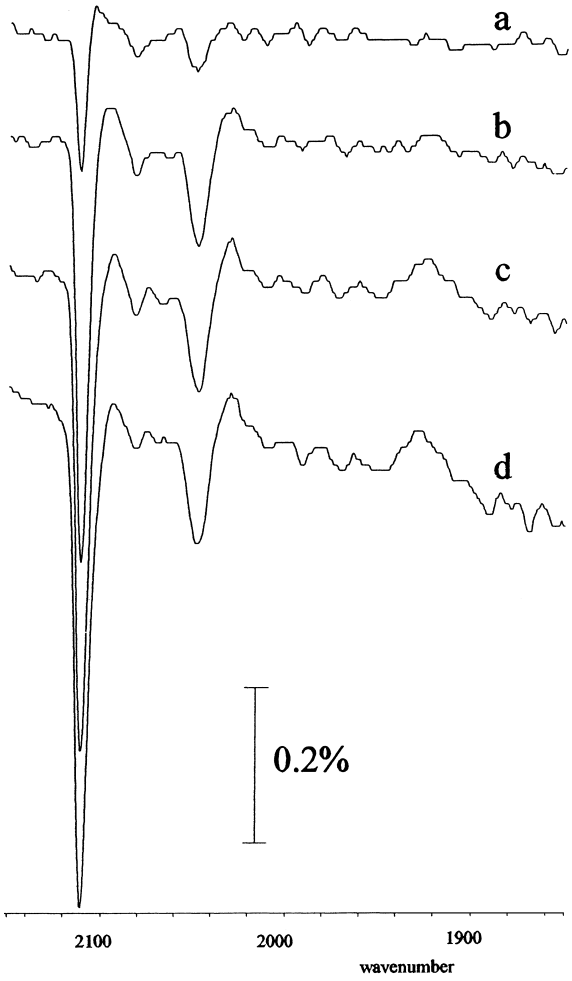

Fig. 2. FT-RAIRS difference spectra, derived from the exposure of TiO_2(1 1 0)–$Rh(CO)_2$ to NO (5×10^{-4} Torr) at room temperature: (a) $<5 \times 10^3$ L; (b) 6×10^4 L; (c) 1.2×10^5 L; (d) 3×10^5 L.

Fig. 3A–C show XPS spectra of the Rh(3d), C(1s), and N(1s) transitions, respectively. Spectra for each of the transitions has been obtained before (a) and after (b) exposure of TiO_2(1 1 0)–$Rh(CO)_2$ to NO at 375 K, and (c) after re-exposure to CO at 375 K. It is clear from the C(1s) spectra that no carbon remains on the surface following NO exposure concomitant with the removal of the gem-dicarbonyl observed in FT-RAIRS (Fig. 2). At the same time the C(1s) signal

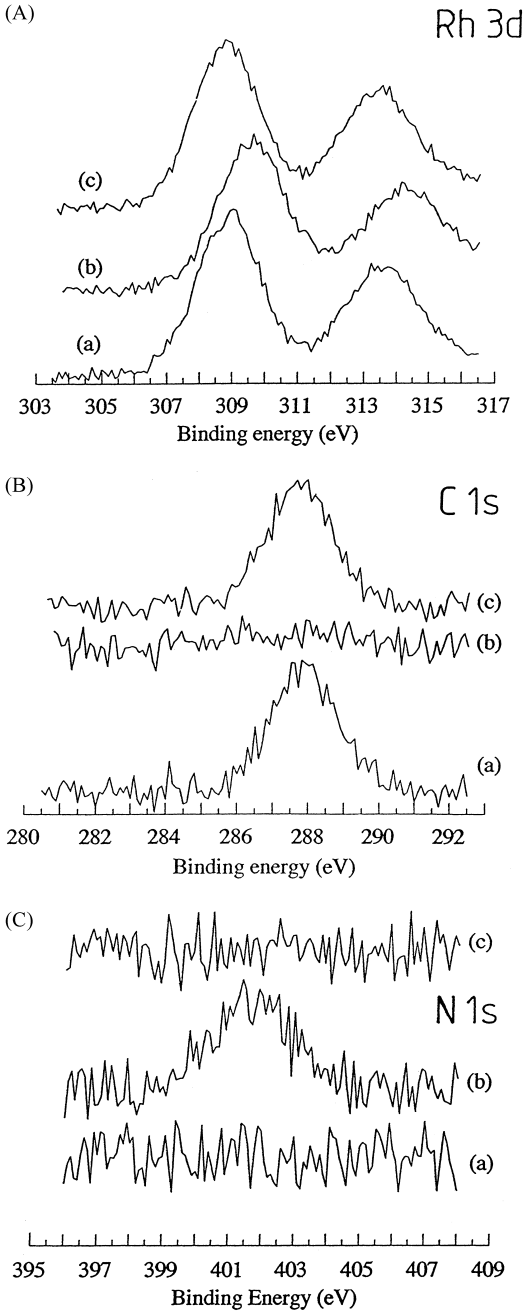

Fig. 3. (A) Rh(3d), (B) C(1s), and (C) N(1s) XPS spectra of: (a) $TiO_2(1\,1\,0)$–$Rh(CO)_2$; (b) after exposure of $TiO_2(1\,1\,0)$–$Rh(CO)_2$ to NO at 375 K; and (c) after re-exposure of the product of (b) to CO at 375 K. The Cl(2p) XPS spectra remained unchanged throughout and is therefore omitted.

is replaced by a peak corresponding to N(1s). Though it is difficult to assign a formal oxidation state to the nitrogen containing species on the basis of the N(1s) binding energy, the value of 402 eV is consistent with an oxidised form of NO rather than a reduced form [40]. If we compare the initial C(1s) intensity due to the geminal dicarbonyl species with that of the N(1s) intensity after reaction, and account for differences in sensitivity factors for N(1s) and C(1s) excitation [40], we obtain a relative stoichiometry in reactant and product of (0.5 ± 0.1):1 for NO:CO. XPS obtained following the exposure to CO of the species produced by the reaction with NO shows complete regeneration of the $TiO_2(1\,1\,0)$–$Rh(CO)_2$ species. The FT-RAIRS and XPS results are therefore consistent with an overall reaction:

$$TiO_2(1\,1\,0)\text{–}Rh(CO)_2 + NO_{(g)} \Leftrightarrow TiO_2(1\,1\,0)\text{–}Rh(NO^+) + 2CO_{(g)} \quad (5)$$

The Cl(2p) XPS (not shown) appears unperturbed throughout the formation of the nitrosyl species and the subsequent regeneration. Previous studies [12,13] concerning the adsorption and chemistry of the $TiO_2(1\,1\,0)$–$Rh(CO)_2$ species, derived from MOCVD of $[Rh(CO)_2Cl]_2$ to the $TiO_2(1\,1\,0)$, have concluded that the Cl atoms on the surface are no longer associated with the Rh centre, and are bound only to the rutile surface. We are, however, unable to say whether the adsorbed Cl atoms influence the forward or reverse reactions outlined in Eq. (5).

The changes in the Rh(3d) spectra observed during the reaction of $Rh(CO)_2$ (Fig. 3) with NO are subtle. The binding energy of the ($3d_{5/2}$) photoelectron line is shifted slightly to *higher* energy by ∼0.2 eV (from 309.1 to 309.3 eV) and the net intensity of the transition is attenuated by a small amount (∼15%) though the width of the line is increased. This is entirely consistent with the FT-RAIRS based deduction that the Rh is still very highly dispersed on the surface and, given the apparent stoichiometry of the reaction (3), it would appear that it is extremely likely that it is still mono-disperse.

Fig. 4A and B show the effects in XPS (C(1s) and N(1s) transitions, respectively) of heating $TiO_2(1\,1\,0)$–$Rh(CO)_2$ and $TiO_2(1\,1\,0)$–$Rh(NO)^+$ produced at 300 K (a) to 500 K (b) and 600 K (c). The $TiO_2(1\,1\,0)$–$Rh(NO)^+$ adduct is thermally more

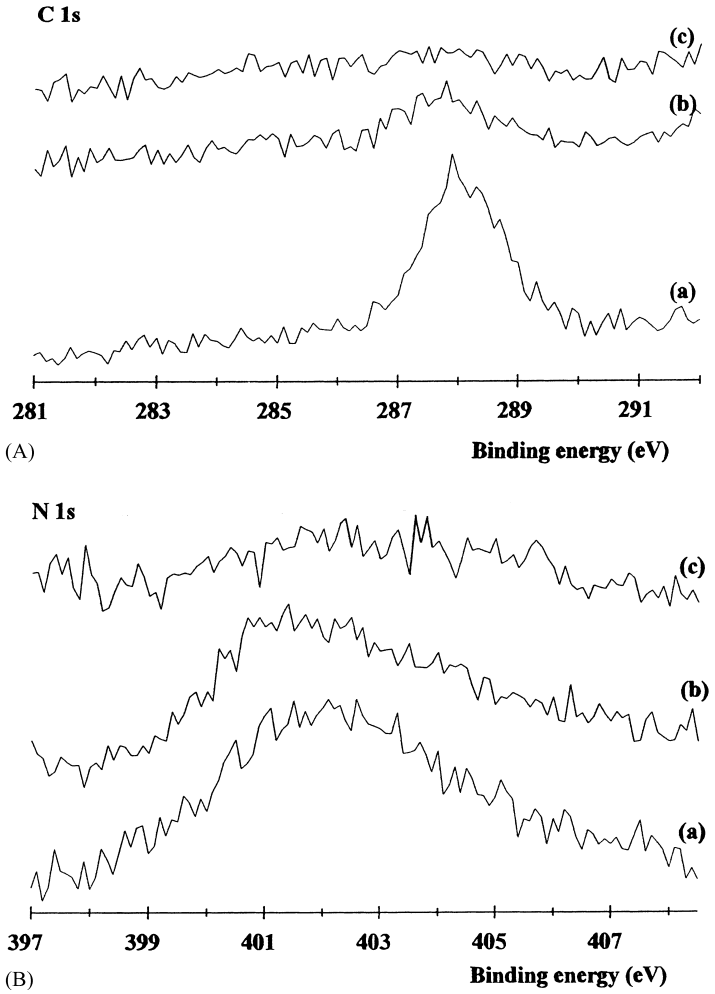

Fig. 4. (A) C(1s) XPS spectra of: (a) TiO_2(1 1 0)–$Rh(CO)_2$ which has subsequently been heated to (b) 500 K and (c) 600 K. (B) N(1s) XPS spectra of (a) TiO_2(1 1 0)–$Rh(NO)^+$ which has subsequently been heated to (b) 500 K and (c) 600 K.

stable than the geminal dicarbonyl species. Moreover, between 500 and 600 K it is thermally removed from the surface without leaving any N residues.

3.3. The reaction of NO with TiO_2(P25)–$Rh(CO)_2$

Fig. 5 shows transmission IR spectra obtained during the exposure of TiO_2(P25)–$Rh(CO)_2$ to NO at 300 K. It can be seen that the reaction observed is somewhat different to that observed on the single crystal. A reduction in the intensity of the geminal dicarbonyl symmetric and asymmetric stretch modes is accompanied by the appearance of a band at 1920 cm^{-1}, and a broad band centred around 1750 cm^{-1}. We also note a differential attenuation of the bands associated with $Rh(CO)_2$: ν_{asym}(C–O) (2030 cm^{-1}) reduces in intensity more than ν_{sym}(C–O) (2110 cm^{-1}). The latter band shifts down in frequency ca. 10 to 2100 cm^{-1} during the reaction with NO.

The band at 1920 cm^{-1} can be unambiguously associated with the formation of TiO_2(P25)–$Rh(NO)^+$ species, as observed in the reaction of NO on TiO_2(1 1 0)–$Rh(CO)_2$. The broad peak centred on 1750 cm^{-1} is more difficult to assign. A band in

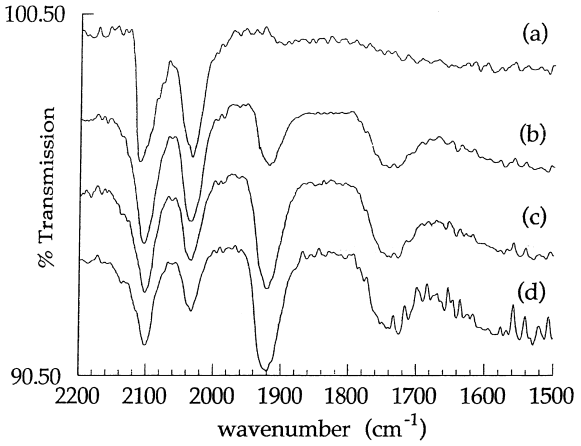

Fig. 5. Transmission IR spectra of (a) TiO_2(P25)–$Rh(CO)_2$ and following exposure to NO (1×10^{-3} Torr) at 300 K; (b) 7×10^5 L; (c) 1.2×10^6 L; (d) 5×10^6 L.

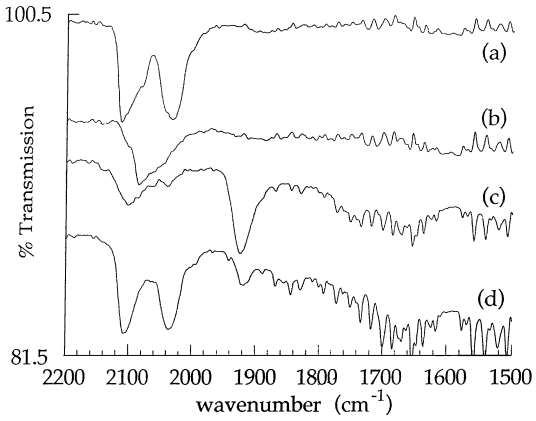

Fig. 6. Transmission IR spectra obtained for: (a) TiO_2(P25)–$Rh(CO)_2$, (b) subsequent to the heating of TiO_2(P25)–$Rh(CO)_2$ to 380 K to produce TiO_2(P25)–Rh^0, (c) exposure of the surface produced in (b) to NO (2.2×10^5 L) at 300 K; and (d) exposure of the product of (c) to CO (3×10^6 L) at 300 K.

this region has previously been assigned (Table 1) to a $Rh(NO)^-$ species, the ν_{asym}(N–O) of a geminal di-nitrosyl species $Rh(NO)_2$, or the ν(N–O) stretch of the mixed geminal species Rh(CO)(NO). In the absence of a corresponding band ν_{sym}(N–O) around 1825 cm^{-1}, which one would expect for $Rh(NO)_2$ [20,25,27,47], we consider it unlikely that this species is formed in the reaction. The persistence of a band at 2100 cm^{-1}, slightly shifted from the ν_{sym}(C–O) stretch of TiO_2(P25)–$Rh(CO)_2$ is most likely associated with the ν(C–O) stretch of the Rh(CO)(NO) species. The band at 1750 cm^{-1} is therefore primarily associated with ν(N–O) of this same species, although an additional contribution to its intensity from a $Rh(NO)^-$ species cannot be excluded.

The reaction of TiO_2(P25)–Rh^0 clusters, formed through the thermal decomposition of TiO_2(P25)–$Rh(CO)_2$ at increasingly high temperatures, was then investigated (Figs. 6–9).

Fig. 6 shows the case where an initially deposited layer TiO_2(P25)–$Rh(CO)_2$ (a) was flashed to ~380 K (b); the resulting surface was then exposed to NO at room temperature (c). Heating to 380 K initiates thermal decomposition of nearly all of the $Rh(CO)_2$ species. Under these conditions one may expect minimal clustering of the supported Rh^0 based on measurements made on the TiO_2(1 1 0) surface [11–14]. There is some evidence of clustering with the observation (Fig. 6b) of a linear CO species on TiO_2(P25)–Rh^0 with ν(C–O) at ~2083 cm^{-1} [13]. Exposure of this surface to NO (Fig. 6c) replaces most of this linearly bound CO with a band in the ν(C–O) region appearing at 2100 cm^{-1}. This we assign to the mixed Rh(CO)(NO) species as observed (above) in the direct reaction of NO with TiO_2(P25)–$Rh(CO)_2$: note there is a weak feature at 1750 cm^{-1}, which is the corresponding ν(N–O) band of this species.

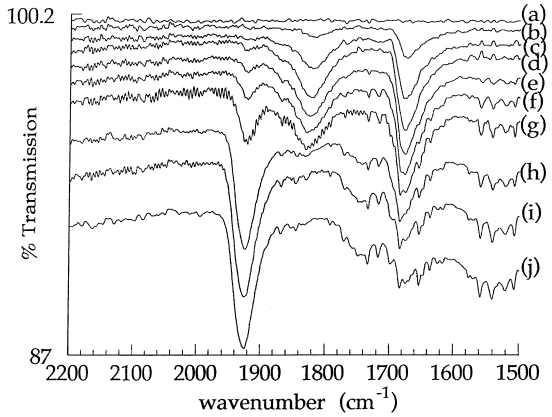

Fig. 7. Transmission IR spectra of TiO_2(P25)–Rh^0 clusters, obtained by heating TiO_2(P25)–$Rh(CO)_2$ to 625 K. TiO_2(P25)–Rh^0 clusters have been exposed to NO at 300 K; (a) 60 L; (b) 360 L; (c) 720 L; (d) 1320 L; (e) 3500 L; (f) 13 300 L; (g) 71 000 L; (h) 3×10^5 L; (i) 1.1×10^6 L; (j) 2×10^6 L.

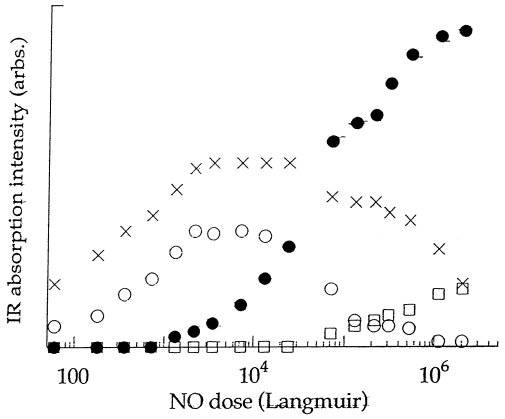

Fig. 8. Integrated absorption intensities for the principal IR bands of the Rh(NO) species observed in Fig. 7: ν(N–O) = 1920 cm^{-1} (filled circles) TiO_2(P25)–Rh(NO)$^+$; ν(N–O) = 1818 cm^{-1} (open circles) linear NO on TiO_2(P25)–Rh^0; ν(N–O) = 1680 cm^{-1} (crosses) bridging NO on TiO_2(P25)–Rh^0; ν(N–O) = 1745 cm^{-1} (squares) Rh(NO)$^-$.

Alongside this we see the appearance (Fig. 6c) of the same dominant feature as were seen in the reaction of NO with TiO_2(P25)–Rh(CO)$_2$ (Fig. 5) at ∼1920 cm^{-1} due to TiO_2(P25)–Rh(NO)$^+$. A notable difference, however, is an additional weak absorption band at ∼1680 cm^{-1}. This we ascribe to NO adsorbed in a bridging configuration [29–31] on a very low concentration of TiO_2(P25)–Rh^0 clusters which have not been disrupted by the NO. Re-exposure of this surface to CO at 300 K (Fig. 6d) results in the conversion of the TiO_2(P25)–Rh(CO)(NO) (ν(C–O) = 2100 cm^{-1} and ν(N–O) = 1750 cm^{-1}) and TiO_2(P25)–Rh(NO)$^+$ (ν(N–O) = 1920 cm^{-1}) species to TiO_2(P25)–Rh(CO)$_2$, but the NO adsorbed on the Rh^0 clusters (ν(N–O) ∼ 1680 cm^{-1}) appears to remain.

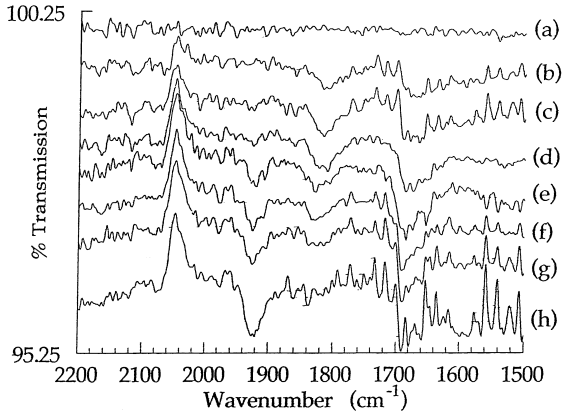

Fig. 9. Transmission IR spectra of TiO_2(P25)–Rh^0 clusters, obtained by heating TiO_2(P25)–Rh(CO)$_2$ to 800 K. TiO_2(P25)–Rh^0 clusters have been exposed to NO at 300 K: (a) 0 L; (b) 60 L; (c) 920 L; (d) 2240 L; (f) 840 L; (f) 14 850 L; (g) 94 500 L; (h) 5.75×10^5 L.

A TiO_2(P25)–Rh^0 surface produced by heating TiO_2(P25)–Rh(CO)$_2$ to 650 K was subsequently exposed to NO at 300 K. At this annealing temperature we expect that CO desorption has been accompanied by significant clustering of the supported Rh [11–14]. We do not expect it to have entered into the SMSI state that can be induced in this system [41–46] although it is likely that some oxygen has decorated the Rh [13]. Fig. 7 is a series of IR spectra obtained on exposing this TiO_2(P25)–Rh surface to NO at 300 K. We note the appearance, and in some cases subsequent disappearance, of a number of bands which we associate with a series of nitrosyl species. The intensities of these bands are plotted in Fig. 8. Initial adsorption of NO produces exclusively two strong bands at 1680 and 1818 cm^{-1}. These bands grow but eventually attenuate above exposures of ca. 5×10^3 L. Concomitant with their disappearance, a strong band at 1920 cm^{-1} grows in intensity, as do weak bands at 1745 and 1550 cm^{-1}.

The band at 1920 cm^{-1} is the easiest to assign in the light of the earlier results, and is associated with the TiO_2(P25)–Rh(NO)$^+$ species. The pair of bands which grow simultaneously at 1680 and 1818 cm^{-1} appear to be associated with an adsorbate which acts as a precursor to the TiO_2(P25)–Rh(NO)$^+$ species: these bands disappear while the 1920 cm^{-1} appears. We have considered the possibility that this precursor is Rh(NO)$_2$, since one may expect the ν_{sym}(N–O) and ν_{asym}(N–O) modes at 1820–1830 and 1740 cm^{-1}, respectively (Table 1). There is, however, a significant difference (60 cm^{-1}) in frequency for the band we observe at 1680 cm^{-1} and ν_{asym}(N–O) of Rh(NO)$_2$. We also considered it unlikely that once formed, Rh(NO)$_2$ would convert to Rh(NO)$^+$ through further exposure of NO at 300 K (Fig. 8). The bands at 1680 and 1818 cm^{-1} are most likely associated with NO adsorbed on the supported Rh^0 clusters. Although NO can dissociate on metallic Rh surfaces, adsorbed molecular NO species have also been observed on

the clean and oxygen covered single crystal surfaces of Rh with bands in the region 1500–1800 cm^{-1} [30–35]. On the basis of results it seems most likely that the bands at 1680 and 1818 cm^{-1} are due to NO in bridged and linear configurations on Rh^0 clusters on the TiO_2(P25). The subsequent disappearance of these bands with NO exposure (Fig. 8) is therefore ascribed to the disruption of the clusters to produce, for example, the TiO_2(P25)–$Rh(NO)^+$ species observed at higher exposures.

The last species to appear, with weak bands at 1745 and 1550 cm^{-1}, are associated (based on previous assignments) with the species TiO_2(P25)–$Rh(NO)^-$ and TiO_2(P25)–$Rh(NO_2)^-$/$Rh(NO_3)^-$, respectively (Table 1). These species are not observed during the reaction of NO with TiO_2(P25)–$Rh(CO)_2$. They are formed either as a result of a reaction of NO with the TiO_2(P25)–Rh^0 clusters, or as a result of a reaction of NO with TiO_2(P25)–Rh^0 or TiO_2(P25)–$Rh(CO)_2$ but specifically in the presence of surface sites which have been created by the thermal treatment. A prime candidate would be oxygen vacancy defects, which could stabilise $Rh(NO)^-$ or $Rh(NO_2)^-$/$Rh(NO_3)^-$.

Fig. 9 shows the effect on the interaction of NO at 300 K with TiO_2(P25)–Rh^0 that has been formed through heating TiO_2(P25)–$Rh(CO)_2$ to 800 K. At this annealing temperature studies indicate that encapsulation of the Rh particles by either O or Ti sub-oxides should occur and the catalyst enter into the SMSI state known for the Rh/TiO_2 system [41–46]. The absorption bands are considerably weaker than in previous experiments. As in the case of the TiO_2(P25)–$Rh(CO)_2$ surface annealed to 650 K (Fig. 7) initial adsorption of NO produces exclusively two bands at 1680 and 1818 cm^{-1}. Whereas these two bands previously disappeared at high exposures (Fig. 9), in this case the band at 1818 cm^{-1} decreases in intensity more slowly at higher exposures, and the band at 1680 cm^{-1} reduces little in intensity. Concomitant with their (less strong) disappearance, a weaker band at 1920 cm^{-1} grows in intensity (Fig. 9). No bands at 1745 and 1550 cm^{-1} are observed.

The appearance of a band at 1920 cm^{-1} indicates that TiO_2(P25)–$Rh(NO)^+$ is again being formed, but at lower concentrations than previously in direct reaction of NO with TiO_2(P25)–$Rh(CO)_2$ or TiO_2(P25)–Rh^0 produced on the surface annealed at 650 K. The association of the two bands at 1680 and 1818 cm^{-1} with NO species adsorbed on the Rh^0 clusters indicates that dispersion of such clusters is less effective for the surface heated to 800 K. Indeed it appears that at the highest exposures such clusters remain covered predominantly with bridged bound NO (Table 1) since the band at 1680 cm^{-1} remains relatively strong (Fig. 9). The observations of changes in nitrosyl band intensities on this surface are again consistent with a model involving conversion of TiO_2(P25)–Rh^0 clusters to TiO_2(P25)–$Rh(NO)^+$, albeit at a lower efficiency. This is most probably associated with the difficulty one may expect in dispersing larger clusters formed at the high annealing temperature (800 K), although inhibition resulting from decoration of the clusters by TiO_x sub oxides cannot be excluded.

Alongside these absorption bands we see a transmission feature growing in with the NO exposure. As a new background has been taken prior to the NO admission and after the flash heating to 800 K this would represent the removal of some species from the surface. Its position would appear to indicate the removal of a linear carbonyl species from the surface. It is likely that after heating some CO from the vacuum background could have adsorbed onto the Rh^0, and that this is subsequently displaced or reacted by the NO.

4. Discussion

4.1. The reaction of NO with TiO_2(1 1 0)–$Rh(CO)_2$

The combination of XPS (Fig. 3) and FT-RAIRS (Fig. 4) results presented here is consistent with TiO_2(1 1 0)–$Rh(CO)_2$ reacting to produce a single product, TiO_2(1 1 0)–$Rh(NO)^+$. Though the detection range of the FT-RAIRS experiment is limited by the InSb detector, the fact that the XPS measurements show the complete removal of carbon species from the surface and a C:N ratio of 2:1 immediately rules out the formation of Rh(CO)(NO) (the ν(C–O) of which we should also be able to detect) or $Rh(NO)_2$. The Rh(3d) peak intensity and position after exposure to NO also rule out the formation of any metallic Rh^0 species and by extension the formation of any NO species supported thereon. It is clear, therefore, that the reaction of NO with the adsorbed TiO_2(1 1 0)–$Rh(CO)_2$ results in the formation of a mono-disperse TiO_2(1 1 0)–$Rh(NO)^+$ species. The

observation of the transmission band (rather than an absorption band) for ν(N–O) is evidence of high dispersion. These two species are therefore associated with the same site on TiO_2(1 1 0), and it therefore seems likely that the same association, made by Srinivas et al. [21] for Rh/SiO_2 catalysts, is correct.

At present, however, we cannot say definitively how this reaction proceeds. This conversion can conceivably be achieved in three ways:

$$TiO_2(1\,1\,0)\text{–}Rh(CO)_2 + 3NO \Leftrightarrow TiO_2(1\,1\,0)\text{–}Rh(NO)^+ + 2CO_{2(g)} + N_{2(g)} \quad (6)$$

$$TiO_2(1\,1\,0)\text{–}Rh(CO)_2 + 5NO \Leftrightarrow TiO_2(1\,1\,0)\text{–}Rh(NO)^+ + 2CO_{2(g)} + N_2O_{(g)} \quad (7)$$

$$TiO_2(1\,1\,0)\text{–}Rh(CO)_2 + NO \Leftrightarrow TiO_2(1\,1\,0)\text{–}Rh(NO)^+ + 2CO_{(g)} \quad (8)$$

We are not able to distinguish between the reactions on the basis of reaction products formed during NO exposure since we are not able to detect these with sufficient sensitivity. The dependence of the rate of the forward reaction at 300 K on NO pressure indicates that the reaction is close to first order in NO, i.e. 100% conversion in 75 min at the rate of 1×10^{-5} Torr versus 100% conversion in ~10 min at the rate of 1×10^{-4} Torr. This suggests that a simple displacement mechanism (8) is most likely to be responsible for the conversion.

The TiO_2(1 1 0)–$Rh(NO)^+$ species is found to have a greater thermal stability than the TiO_2(1 1 0)–$Rh(CO)_2$ species (Fig. 4A and B), which is consistent with the observation that the Rh–N bond is stronger than the Rh–C bond in similar systems. Whilst we cannot carry out any quantitative kinetic analysis on the basis of the XPS measurements, the results show that the thermal decomposition of this species occurs cleanly with no residual N species persisting above 600 K.

The association of the new adsorption band at ~1920 cm^{-1} with the formation of a $Rh(NO)^+$ species is based mainly upon previous assertions made in the literature for supported systems. These in turn have been based upon IR measurements made upon inorganic nitrosyls for which diffraction studies have definitively determined the Rh–NO bond angle. Whilst, on the basis of current measurements we cannot affirm the linearity of this bond explicitly, we may make suggestions regarding the nature of this species supported upon the single crystal surface. Firstly we note that our XPS measurements, assuming dominated by initial state effects, would indicate that the oxidation state of the Rh rather similar in both geminal dicarbonyl and $Rh(NO)^+$ case. We have also noted the stability of the nitrosyl species in relation to the geminal dicarbonyl. This suggests that the Rh centre in TiO_2(1 1 0)–$Rh(NO)^+$ has not been reduced by the addition of NO, and that it remains in an (approximately) +1 state. In order to maintain charge balance, we suggest that the stoichiometric and defect free TiO_2(1 1 0) surface is effectively electron deficient (Lewis acid), perhaps resulting from the presence of five co-ordinate Ti atoms. The fate of the extra electron provided by the NO is to be transferred into the surface to compensate for the net electron deficiency of TiO_2(1 1 0).

4.2. The reaction of NO with TiO_2(P25)–$Rh(CO)_2$

A similar IR band similar to that observed on TiO_2(1 1 0)–$Rh(CO)_2$ is observed at 1920 cm^{-1} on TiO_2(P25)–$Rh(CO)_2$ during exposure to NO (Fig. 5), and is evidence that a primary product in the reaction at 300 K is TiO_2(P25)–$Rh(NO)^+$. In contrast to the reaction of NO with TiO_2(1 1 0)–$Rh(CO)_2$, the species TiO_2(P25)–Rh(NO)(CO) is also produced during the reaction of NO with TiO_2(P25)–$Rh(CO)_2$. This is evident from the bands at 2100 and 1750 cm^{-1} assigned to ν(C–O) and ν(N–O), respectively. It would appear that this species is not a precursor to the formation of completely decarbonylated TiO_2(P25)–$Rh(NO)^+$ species as it co-exists with the other Rh(NO) states and does not react further with NO. The absence of such a species on TiO_2(1 1 0) would indicate that the formation of this species is either specific to the surfaces of anatase (some may remain after the annealing procedure), or simply the result of structure sensitivity in the chemistry on rutile; i.e. it is formed on surface planes other than rutile (1 1 0).

Common to experiments on TiO_2(1 1 0) and TiO_2(P25) is the relative facility of the reaction of NO with supported geminal dicarbonyl with respect to the reverse regeneration reaction. The former reaction appears to be much easier; orders of magnitude less NO being required to convert the geminal species to the

various supported Rh(NO) adducts than is required to return these species to the geminal dicarbonyl state.

4.3. The reaction of NO with TiO_2(P25)–Rh^0

The reaction of NO with TiO_2(P25)–Rh^0 produced by the thermal treatment of TiO_2(P25)–$Rh(CO)_2$ exhibits a dependence on the annealing temperature. Heating the surface to 380 K (Fig. 6) is sufficient to partly desorb CO from TiO_2(P25)–$Rh(CO)_2$ and produce clusters of TiO_2(P25)–Rh^0 on which CO is adsorbed. Exposure of these clusters, and the remaining TiO_2(P25)–$Rh(CO)_2$, to NO produces the products one may expect (see above) for the reaction with TiO_2(P25)–$Rh(CO)_2$, i.e. TiO_2(P25)–$Rh(NO)^+$ and TiO_2(P25)–Rh(NO)(CO). In addition bridged NO is observed (ν(N–O) $\sim$ 1680 cm^{-1}) [29–31] on what appear to be a small proportion of TiO_2(P25)–Rh^0 clusters which remain intact. While the TiO_2(P25)–$Rh(NO)^+$ and TiO_2(P25)–Rh(NO)(CO) are easily reconverted to TiO_2(P25)–$Rh(CO)_2$ on re-exposure to CO (Fig. 6), the TiO_2(P25)–Rh^0 clusters remain covered with adsorbed bridging NO.

The reaction of NO with TiO_2(P25)–Rh^0 produced by heating TiO_2(P25)–$Rh(CO)_2$ to 650 K (Figs. 7 and 8) produces a complex sequence of inter-conversions between the supported Rh(NO) products. The clusters are sufficiently large and robust that initial exposure to NO results in the adsorption of bridged and linear NO species on TiO_2(P25)–Rh^0 (ν(N–O) $\sim$ 1680 and 1818 cm^{-1}, respectively). It is likely that a proportion of the adsorbing NO dissociates on the metallic clusters, and that these bands may be due to species perturbed by the dissociation products, adsorbed N and O. No dispersed Rh nitrosyl species are observed during the initial NO exposure. The adsorption of NO on TiO_2(P25)–Rh^0 clusters is followed by their re-dispersion at 300 K to form TiO_2(P25)–$Rh(NO)^+$ as evidenced by the strong growth of the band at 1920 cm^{-1} concomitant with the disappearance of the bands associated with NO on TiO_2(P25)–Rh^0. The last species to appear during exposure to NO, with weak bands at 1745 and 1550 cm^{-1} we have assigned to TiO_2(P25)–$Rh(NO)^-$ and TiO_2(P25)–$Rh(NO_2)^-/Rh(NO_3)^-$ species, respectively (Table 1). These species were not observed during the reaction of NO with TiO_2(P25)–$Rh(CO)_2$. One possibility is that they can be formed only as a result of the re-dispersion reaction of NO with the TiO_2(P25)–Rh^0 clusters. However, it can be seen from Fig. 8 that this does not take place during initial dispersion which results in the formation of exclusively TiO_2(P25)–$Rh(NO)^+$. We suggest that a more likely requirement for the formation of to TiO_2(P25)–$Rh(NO)^-$ or TiO_2(P25)–$Rh(NO_2)^-/Rh(NO_3)^-$ is a reaction (perhaps via the formation of TiO_2(P25)–$Rh(NO)^-$) of NO with TiO_2(P25)–Rh^0 specifically in the presence of surface defect sites which have been created by the thermal treatment. A prime candidate would be oxygen vacancy defects, which we suggest could stabilise $Rh(NO)^-$ or $Rh(NO_2)^-/Rh(NO_3)^-$. A possible mechanism for this is the co-ordination of the Rh at a defect site where negative charge is expected to stabilise the surface structure (missing oxygen atom). Similar Rh(NO) species have been seen previously and postulated as being a mono-disperse, and it is worthy of note that this has recently been confirmed for a similar species observed on high area $Rh(CO)_2/Al_2O_3$ and $Rh(CO)_2/TiO_2$ systems (also produced through the $[Rh(CO)_2Cl]_2$ precursor) [48] following reaction with NO at 300 K.

Annealing to surface temperatures of 800 K produces TiO_2(P25)–Rh^0 clusters onto which the chemisorption of NO at 300 K is strongly suppressed (Fig. 9), as one may expect with the onset of SMSI characteristic of the Rh/TiO_2 system under these conditions [41–46]. As in the case of TiO_2(P25)–Rh^0 produced by annealing at 650 K (Fig. 7), initial adsorption of NO produces exclusively two bands at 1680 and 1818 cm^{-1}, although they are significantly weaker. Further, whereas these two bands previously disappeared at high exposures (Figs. 7 and 8), in this case the band at 1818 cm^{-1} decreases in intensity much more slowly, and the band at 1680 cm^{-1} reduces little in intensity. Concomitant with their (less strong) disappearance, a weaker band at 1920 cm^{-1}, associated with the mono-dispersed species $Rh(NO)^+$, grows in intensity (Fig. 9). Re-dispersion of TiO_2(P25)–Rh^0 is clearly considerably curtailed for clusters produced at the higher annealing temperature of 800 K. The increased size of clusters produced at 800 K, or their encapsulation by TiO_2 sub-oxides, must be responsible for the hindrance in re-dispersion.

We also have noted that for clusters produced at 800 K, no bands at 1745 and 1550 cm^{-1} are observed during re-dispersion. This may also be due to the

limited dispersing power of NO for such particles, or a lower concentration of defects following the annealing treatment if these are responsible for the stabilisation of $Rh(NO)^-$ or $Rh(NO_2)^-/Rh(NO_3)^-$ as suggested above.

5. Conclusions

5.1. The reaction of NO with TiO_2(1 1 0)–$Rh(CO)_2$

TiO_2(1 1 0)–$Rh(CO)_2$, formed from the dissociation $[Rh(CO)_2Cl]_2$, is converted through reaction with NO at 300 K to a highly dispersed $Rh(NO)^+$ species. A transmission band associated with ν(N–O) of this species is observed in FT-RAIRS at 1920 cm^{-1}. This species is thermally more stable than the geminal dicarbonyl species and XPS measurements indicate that the NO is removed without nitrogen residues by 600 K.

Exposure of TiO_2(1 1 0)–$Rh(NO)^+$ to CO at 300 K results in the complete regeneration of TiO_2(1 1 0)–$Rh(CO)_2$. Both this regeneration process, and the synthesis of the TiO_2(1 1 0)–$Rh(NO)^+$, are found to be facilitated by increased temperature (up to ∼400 K) though the regeneration reaction is significantly more difficult.

5.2. The reaction of NO with TiO_2(P25)–$Rh(CO)_2$

MOCVD of $[Rh(CO)_2Cl]_2$ on titania powder (Degussa 25) at 300 K results in the adsorption of TiO_2(P25)–$Rh(CO)_2$ in a variety of surface environments, with broad bands observed at the same frequencies as on TiO_2(1 1 0) for ν_{sym}(C–O) at 2110 and ν_{asym}(C–O) at 2030 cm^{-1}. Exposure of TiO_2(P25)–$Rh(CO)_2$ to NO at 300 K results in the formation of TiO_2(P25)–$Rh(NO)^+$ with ν(N–O) at 1920 cm^{-1}, and TiO_2(P25)–Rh(CO)(NO) with ν(N–O) at 1750 cm^{-1} and ν(C–O) at 2110 cm^{-1}.

5.3. The reaction of NO with TiO_2(P25)–Rh^0 clusters

Surfaces on which a variety of TiO_2(P25)–Rh^0 clusters have been formed through the thermal decomposition of TiO_2(P25)–$Rh(CO)_2$ at various temperatures react with NO to produce additional surface nitrosyl species. We find, however, no evidence for the formation of a $Rh(NO)_2$ species in this system whereas on Al_2O_3 [20,25,27] and systems based on zeolite-Y [47] it has often been invoked.

On a surface heated to 380 K, where TiO_2(P25)–$Rh(CO)_2$ decarbonylation has only just taken place, reaction with NO at 300 K results in the same species as that produced through the reaction of NO directly with TiO_2(P25)–$Rh(CO)_2$ i.e. TiO_2(P25)–$Rh(NO)^+$ and TiO_2(P25)–Rh(CO)(NO). In contrast with the reaction with larger clusters, no precursor species are observed. This is either because the TiO_2(P25)–Rh^0 formed at 380 K is mainly mono-dispersed, or the clusters are very small and the reaction is very fast. Under these conditions, a small amount of bridging NO is observed (ν(N–O) at 1680 cm^{-1}), and this species is associated with a low concentration of TiO_2(P25)–Rh^0 clusters which remain intact during NO exposure. Re-exposure of this surface to CO results in the complete re-conversion of the dispersed nitrosyl species TiO_2(P25)–$Rh(NO)^+$ and TiO_2(P25)–Rh(CO)(NO) back to TiO_2(P25)–$Rh(CO)_2$, while bridging NO species are not displaced from the TiO_2(P25)–Rh^0 clusters.

On a surface heated to 650 K where TiO_2(P25)–$Rh(CO)_2$ decarbonylation has taken place and larger TiO_2(P25)–Rh^0 clusters have been formed, probably decorated with adsorbed oxygen [13], reaction with NO leads initially to the adsorption of linear and bridged bound NO on TiO_2(P25)–Rh^0 with respective ν(N–O) bands observed in the IR at 1818 and 1680 cm^{-1}. Further exposure of NO, however, results in the disruption of the TiO_2(P25)–Rh^0 clusters. This is evidenced by the disappearance of the bridging and linear bands and the appearance of a strong band associated with ν(N–O) of TiO_2(P25)–$Rh(NO)^+$ at 1920 cm^{-1}. In addition, at the highest exposures of NO, bands at 1745 and 1550 cm^{-1} are observed and assigned to dispersed TiO_2(P25)–$Rh(NO)^-$ and TiO_2(P25)–$Rh(NO_2)^-/(NO_3)^-$. The latter species, which were not observed following the reaction of NO with TiO_2(P25)–Rh^0 produced at 380 K, we suggest are stabilised by surface defects such as oxygen vacancies. These may have been formed during the clustering of the Rh^0 [13].

After thermal treatment of TiO_2(P25)–$Rh(CO)_2$ to temperatures of 800 K, where encapsulation of the TiO_2(P25)–Rh^0 clusters should occur, we see a strong

suppression of NO adsorption on the clusters. Nevertheless disruption of clusters still takes place with the formation of TiO_2(P25)–Rh(NO) even under these (SMSI) conditions.

Acknowledgements

We would like to thank EPSRC for the provision of postgraduate and postdoctoral fellowships to AK and MAN, respectively, and Huntington-Brae at AWE for support for NY.

References

[1] L. Guczi (Ed.), Studies in Surface Science and Catalysis, Vol. 64, Elsevier, Amsterdam, 1991.
[2] P. Johnston, R.W. Joyner, in: T.J. Dines, C.H. Rochester, J. Thomson (Eds.), Catalysis and Surface Characterisation, Royal Soc. Chem., 1992, p. 51.
[3] P. Johnston, R.W. Joyner, P.D.A. Pudney, E.S. Shpiro, B.P. Williams, Faraday Dis. Chem. Soc. 89 (1990) 144.
[4] P. Johnston, R.W. Joyner, J. Chem. Soc., Faraday Trans. 89 (1993) 863.
[5] S.D. Jackson, B.J. Brandreth, D. Winstanley, J. Chem. Soc., Faraday Trans. 84 (1988) 1741.
[6] A.C. Yang, C.W. Garland, J. Phys. Chem. 61 (1957) 1504.
[7] J.T. Yates, T.M. Duncan, S.D. Worley, R.W. Vaughan, J. Chem. Phys. 70 (1979) 1219.
[8] F. Solymosi, M. Pastor, J. Phys. Chem. 89 (1985) 4789.
[9] T.H. Ballinger, J.T. Yates, J. Phys. Chem. 95 (1991) 1694.
[10] J.T. Yates, K. Kolasinski, J. Chem. Phys. 79 (1983) 1026.
[11] J. Evans, B.E. Hayden, F. Mosselmans, A. Murray, J. Am. Chem. Soc. 114 (1992) 6912.
[12] J. Evans, B.E. Hayden, F. Mosselmans, A. Murray, in: R.W. Joyner, R.A. Van Santen (Eds.), Elementary Reaction Steps in Heterogeneous Catalysis, Nato ASI Series, 1993, p. 179.
[13] J. Evans, B.E. Hayden, F. Mosselmans, A. Murray, Surf. Sci. 301 (1994) 61.
[14] J. Evans, B.E. Hayden, F. Mossehnans, A. Murray, Surf. Sci. Lett. 279 (1992) L159.
[15] B.E. Hayden, A. King, M.A. Newton, Surf. Sci. 397 (1998) 306.
[16] B.E. Hayden, A. King, M.A. Newton, Chem. Phys. Lett. 269 (1997) 485.
[17] C.D. Meyer, R. Eisenberger, J. Am. Chem. Soc. 98 (1976) 1364.
[18] H.C. Yao, Y.F. Yu-Yao, K. Otto, J. Catal. 56 (1979) 21.
[19] S.E. Oh, C.C. Eickel, J. Catal. 128 (1991) 526.
[20] F. Solymosi, T. Bansagi, E. Novak, J. Catal. 112 (1988) 183.
[21] G. Srinivas, S.S.C. Chang, S. Debnath, J. Catal. 148 (1994) 748.
[22] E. Novak, D. Sprinceana, F. Solymosi, Appl. Catal. A 149 (1997) 89.
[23] K.C. Cannon, S.K. Ho, J.M. White, J. Am. Chem. Soc. 111 (1989) 5064.
[24] F. Solymosi, J. Sarkany, Appl. Surf. Sci. 3 (1979) 68.
[25] E.A. Hyde, R. Rudham, J. Chem. Soc., Faraday Trans. 80 (1984) 531.
[26] H. Arai, H. Tominaga, J. Catal. 43 (1976) 131.
[27] J. Liang, H.P. Wang, L.D. Spicer, J. Phys. Chem. 89 (1985) 5840.
[28] R. Dictor, J. Catal. 109 (1988) 89.
[29] T.W. Root, G.B. Fisher, L.D. Schmidt, J. Chem. Phys. 85 (1986) 4879.
[30] G. Cautero, C. Astaldi, P. Rudolf, M. Kishkinova, R. Rosei, Surf. Sci. 258 (1991) 44.
[31] J.S. Villarubia, W. Ho, J. Chem. Phys. 87 (1987) 750.
[32] H.J. Borg, J.F.C.-J.M. Reijerse, R.A. Van Santen, J.W. Niemantsverdriet, J. Chem. Phys. 101 (1994) 10052.
[33] Y.J. Kim, S. Thevuthasan, G.S. Herman, C.H.F. Peden, S.A. Chambers, D.N. Belton, H. Permana, Surf. Sci. 359 (1996) 269.
[34] D.J. Loffreda, D. Simon, P. Sautet, Chem. Phys. Lett. 291 (1998) 15.
[35] T.W. Root, G.B. Fisher, L.D. Schmidt, J. Chem. Phys. 85 (1986) 4687.
[36] P. Basu, T.H. Ballinger, J.T. Yates Jr., Rev. Sci. Instr. 59 (1988) 1321.
[37] J.C.S. Wong, J.T. Yates Jr., J. Phys. Chem. 99 (1995) 12640.
[38] J.C.S. Wong, J.T. Yates Jr., J. Am. Chem. Soc. 116 (1994) 1610.
[39] Y. Chabal, Surf. Sci. Rep. 8 (1988) 301.
[40] D. Briggs, M.P. Seah (Eds.), Practical Surface Analysis by X-Ray Photoelectron Spectroscopy, Wiley, New York, 1990.
[41] G.L. Haller, D.E. Resasco, Adv. Catal. 36 (1989) 173.
[42] G.L. Haller, D.E. Resasco, J. Catal. 82 (1983) 279.
[43] V. Vishwanathan, S. Narayanan, Catal. Lett. 21 (1993) 183.
[44] S. Bernal, F.J. Botana, J.J. Calvino, C. Lopez, J.A. Perez-Omil, J.M. Rodriguez-Izquerido, J. Chem. Soc., Faraday Trans. 92 (1996) 2799.
[45] D.C. Koningsberger, J.H.A. Martens, R. Prins, D.R. Short, D.E. Sayers, J. Phys. Chem. 90 (1986) 3047.
[46] A. Berko, I. Ulrych, K.C. Prince, 102 (1998) 3379.
[47] T. Iizuka, J.H. Lunsford, J. Mol. Catal. 8 (1980) 391.
[48] D.G. Burnaby, A.J. Dent, S. Diaz-Moreno, J. Evans, S.G. Fiddy, T. Neisius, M.A. Newton, S. Turin, in preparation.